Novel Synthesis of Manganese Spinel Nanoparticles via Combustion with Mn^{III}(acac)$_3$ as Precursor

Mehdi Salehi[*] **and Fatemeh Ghasemi**

Department of Chemistry, Faculty of Sciences, Semnan University, Semnan, I. R. Iran.

(*) Corresponding author: msalehi@semnan.ac.ir

Abstract

In the present work Mn$_3$O$_4$ nanoparticles (NPs) with spinel structure were synthesized successfully via combustion route with MnIII(acac)$_3$ as precursor in two different temperatures. The morphology of the synthesized Mn$_3$O$_4$ were investigated by field emission scanning electron microscope (FESEM) and structural analysis was studied by powder X-ray diffraction (PXRD) technique that it indicated that the Mn$_3$O$_4$ nanoparticles with space group of l41/amd Structural analysis was performed by fullprof program employing profile matching with constant scale factors. The lattice parameters for both samples were found a = b = 5.7621 Å and c= 9.4696 Å, α = β = γ = 90°. In addition, the size of the Mn$_3$O$_4$ nanoparticles obtained from the Transmission Electron Microscopy (TEM) that the average is 20 nm. Magnetic property of synthesized Mn$_3$O$_4$ was done by Vibration Sampling Magnetometer (VSM) that confirm the paramagnetic behavior. The optical properties of the obtained materials were investigated by Furrier-Transform Infrared spectroscopy (FTIR) and Ultraviolet-Visible spectrum (UV-Vis). The thermal stability was determined by Thermo Gravimetric Analysis (TGA).

Keywords: *Mn$_3$O$_4$ Nanoparticles, Combustion Method, FESEM, Spinel, TEM.*

1. INRODUCTION

Investigation on Nanomaterials has been interested by researchers because of their interesting properties compared with their corresponding bulk structure. Mn$_3$O$_4$ is one of the most stable oxides of manganese. It is a magnetic transition metal, and is known as an effective and inexpensive catalyst in various oxidation and reduction reactions. It has normal spinel structure were the oxide ions are cubic closed packed and the Mn(II) occupies the tetrahedral sites and Mn(III) occupies the octahedral sites. The structure is distorted due to a Jahn-Teller effect [1, 2]. Mn$_3$O$_4$ has paramagnetic behavior at room temperature and it is ferromagnetic under 41-43 K [3]. They have tremendous potential in a large number of applications, such as catalysis [4-8], electrode materials, [9, 10] and magnetic storage devices [11]. Nano-sized Mn$_3$O$_4$ is also used as main sources of ferrite materials [12] and widely used as the active material of electrodes in many alkaline rechargeable batteries, especially in the lithiation of Li–Mn–O electrode materials for rechargeable lithium batteries [13, 14] and It can be used as the precursor of catalysts [15]. Various methods have been recorded for the preparation of nanocrystalline Mn$_3$O$_4$ powders such as chemical bath deposition [16], solvothermal [17, 18], co-precipitation [19], microwave irradiation [20], and surfactant-assisted methods [21]. The present study reports combustion method for synthesis of Mn$_3$O$_4$, which is considered as a simple and efficient method among them. The powder able to combust organic compounds in the temperature range of 100–500 °C, and can be used for the selective reduction of nitrobenzene [22, 23]. In this paper, we have prepared Mn$_3$O$_4$ nanocrystals by using some simple combustion methods (Figure 1.) using a complex without fuel. We have also used an oven and

characterized the prepared samples by carrying out X-ray diffraction, scanning electron microscopy, energy dispersive X-ray spectroscopy and electrochemical measurements. To the best of our knowledge, there is no report on the synthesis of Mn_3O_4 by this method.
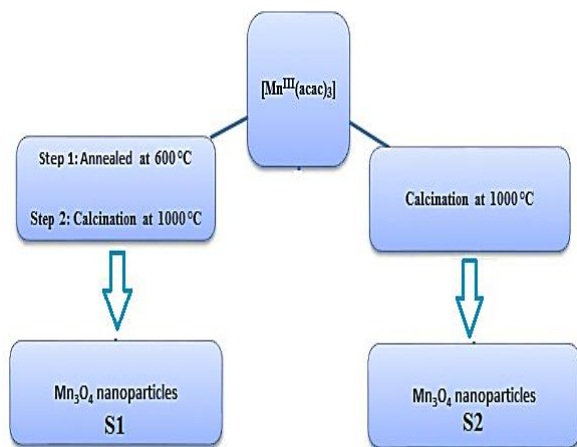
Figure 1. *Mn_3O_4 nanoparticles synthesis process.*

2. EXPERIMENTAL
2.1. General Remark

All chemicals were of analytical grade, obtained from commercial sources, and used without further purifications. Phase identifications were performed on a powder X-ray diffractometer D5000 (Siemens AG, Munich, Germany) using CuKα source. The morphologies of the obtained materials were examined with a field emission scanning electron microscope (Hitachi FE-SEM model S-4160. Mn_3O_4 particles were dispersed in water and cast onto a copper grid to study the sizes and morphology of the particles by TEM (Transmission Electron Microscopy) using a Philips-CM300-150 KV microscope. FTIR spectra were recorded on FT-IR SHIMADZU. UV-Vis studies were done by UV-1650PC SHIMADZU. Magnetic property studies were recorded by Vibration Sampling Magnetometer (Model 7400 VSM). The sample was measured from -10 kOe to +60 kOe at room temperature.

2.2. Synthesis of Complexes [$Mn^{III}(acac)_3$]:

First of all 0.52 g of manganese (II) chloride tetra hydrate and 1.4 g of sodium acetate were dissolved in 20 mL of distilled water. A solution of 0.11 g of potassium permanganate in 6 mL of distilled water was prepared. The obtained solution was stirred until $KMnO_4$ was being dissolved. Then $KMnO_4$ solution had been added drop wise for 10-15 minutes to the reaction mixture. It was stirred for further 10 minutes and then a solution of 1.4 g of sodium acetate was added drop-wise in 5 mL of distilled water. While stirring, the resulted dark mixture was heated in a water bath at 60 °C to 70 °C for 15 minutes. A black color product was filtered and washed by approximately 10 mL of cold distilled water. It was vacuum dried for 15 minutes. Yield of reaction was 85%.

2.3. Synthesis of Mn_3O_4 Nanoparticles

To investigate the effects of temperature on the size of the nanoparticles, it is used two different conditions of temperature to produce nanoparticles. For synthesizing first sample (S_1) certain amounts of the $Mn^{III}(acac)_3$ was transferred into a crucible. Then the crucible was transferred into a preheated oven at 600 °C and was annealed for 3 h and after the reaction was completed, the crucible was cooled to the room temperature normally. In the next step the reaction product was calcinated at 1000 °C for 3h, then cooled normally to 25 °C.

For synthesizing second sample (S_2) certain amounts of $Mn^{III}(acac)_3$ added into a crucible, then it was transferred into a preheated oven at 1000 °C and was calcined directly at this temperature for 3 h. At the end, the final product was cooled to the room temperature normally. Finally the red colored powders was obtained.

3. RESULTS AND DISCUSSION
3.1. FT-IR Analysis

FT-IR analysis was performed to investigate the surface characteristics of

the prepared samples and the precursor spectra which are presented in figure 2. The vibrations of ions in the crystal lattice are usually observed in the range of 400 ~ 1000 cm^{-1} in FT-IR analysis. In the region from 400 to about 500 cm^{-1}, two absorption peaks were observed at 424 and 530 cm^{-1} which may be associated with the coupling of the Mn-O stretching modes of tetrahedral and octahedral sites, as expected from a normal spinel structure.

Actually the vibration frequency located at 530 cm^{-1} can be corresponded to the distortion vibration Mn-O in an octahedral environment. The strong peak at 632 cm^{-1} is characteristic of hausmannite with a spinel structure, corresponding to the Mn-O stretching vibration of divalent manganese ions in the tetrahedral coordination.
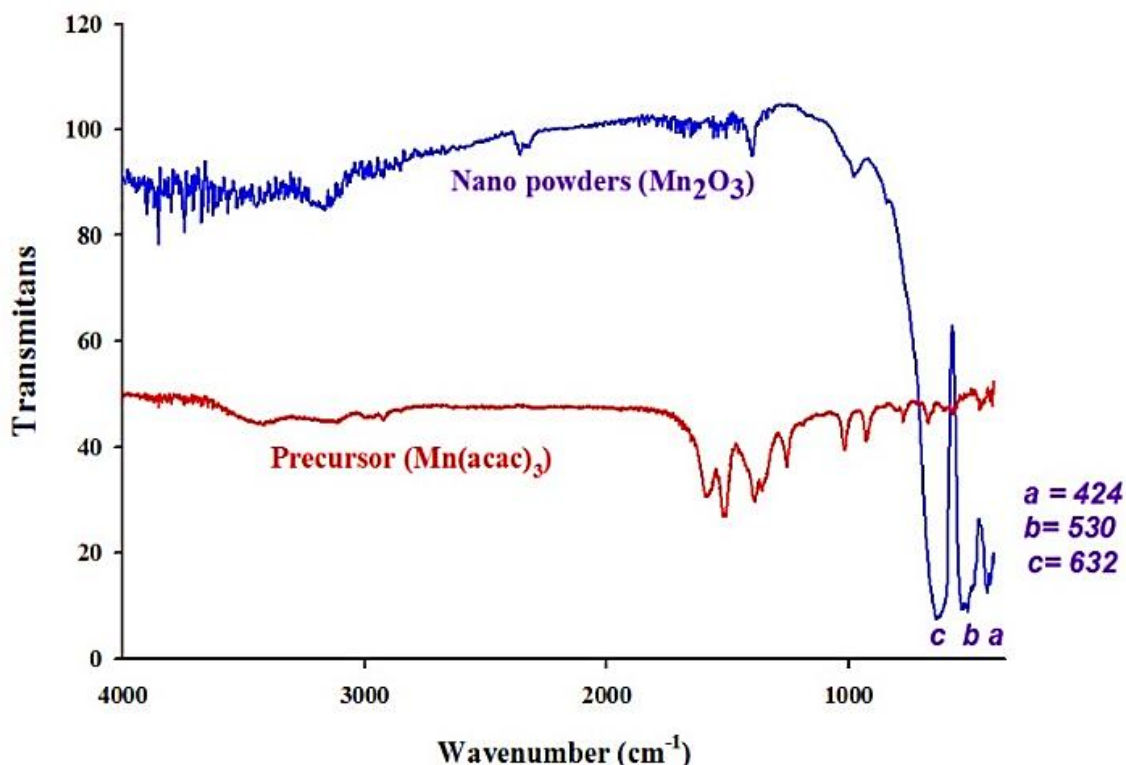

Figure 2. *FT-IR spectra of the synthesized Mn_3O_4 nanoparticles and $Mn^{III}(acac)_3$ as precursor.*

3.2. UV–Vis Spectra

The UV–Vis spectra of the synthesized materials of Mn_3O_4 (S_1, S_2) are given in Figure 3. The bands at 222, 280 and 370 nm are attributed to the allowed $O^{-2} \rightarrow Mn^{+2}$ (the two former) and $O^{-2} \rightarrow Mn^{+3}$ (the latter) charge transfer transitions, respectively. This spectrum is typical of the hausmannite phase.

S_1 (b)

S_2 (c)

S_2 (d)
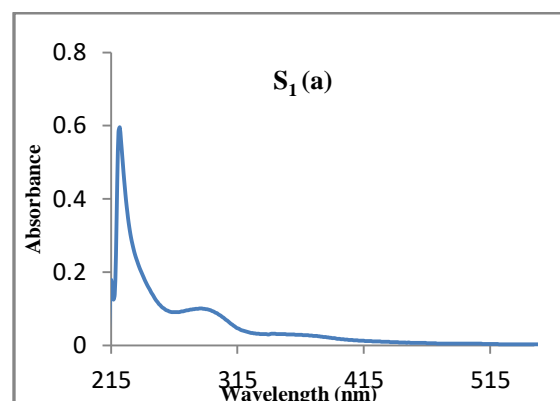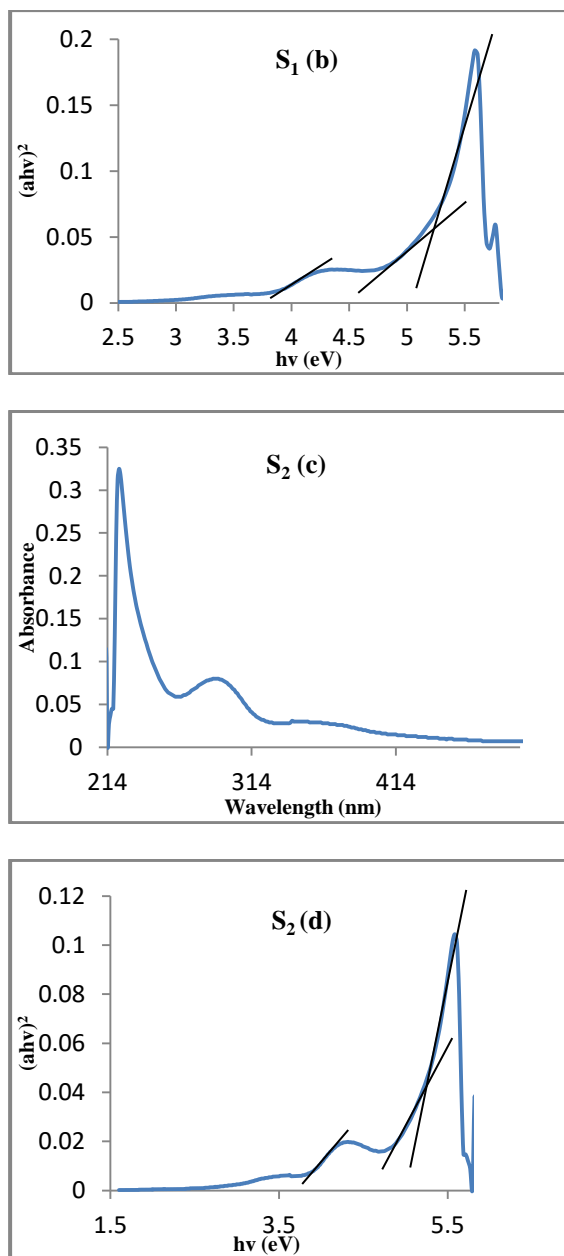
Figure3. *UV-Vis electronic absorption of S_1 and S_2 where $S_1(a)$ and $S_2(c)$ are UV-Vis absorption spectra; and $S_1(b)$ ad $S_2(d)$ are the $(\alpha h\nu)^2$ versus $h\nu$ plots.*

3.3. XRD Analysis

Crystal phases of the as-synthesized materials were analyzed by using powder X-ray diffraction (PXRD) technique. Figures 4a and 4b show PXRD pattern of as-prepared Mn_3O_4 nanoparticles as data points. The results of structural analysis performed throughout the FullProf program by employing profile matching analysis (full line) with constant scale factors are also included. Red bars are the observed intensities while the black ones are the calculated data. The blue one is the difference: $Y_{obs}-Y_{calc}$. The XRD patterns showed that the synthesized nanomaterials were crystallized in a tetragonal crystal structure, with space group of l41/amd (JCPDS 24-0734). The lattice parameters were found as a = b = 5.7621 Å, c = 9.4696 Å with α = β = γ = 90° For all the prepared samples, diffraction peaks located at 17.95, 28.94, 31.02, 36.136, 38.004, 44.43, 50.72 , 58.53 and 59.84 °, which can be perfectly attributed to peaks with the following miller indices: (101), (112), (103), (211), (004), (220), (105), (321), and (224) crystallographic planes of the tetragonal Mn_3O_4. Table 1 shows the cell parameter refinement data for S_1 and S_2. It was found that by changing the reaction conditions, the volume of the unit cell was increased. So there is a contraction in the unit cell with increasing temperature concentration for the synthesis of Mn_3O_4.

3.4. Microstructural Studies

For analyzing the morphology of the synthesized materials it was used FESEM and TEM. Figure 5 shows FESEM image of S_1 (a, b) and S_2 (c, d). also it shows that the synthesized nanomaterial had sphere-like morphology and the diameter size of the synthesized nanomaterials were in the range of about 20-40 nm. It seems that the lower temperature, cause to smaller particle size.

Also for precious investigation of the size and morphology of obtained material S_1 and S_2 are used TEM image in various magnification in Figure 6 (a-d).

It shows the particle size is about 20 nm also, a strong agglomeration and high transparency under TEM is obvious for S_1. This image emphasis the square and hexagonal sheet like morphology.
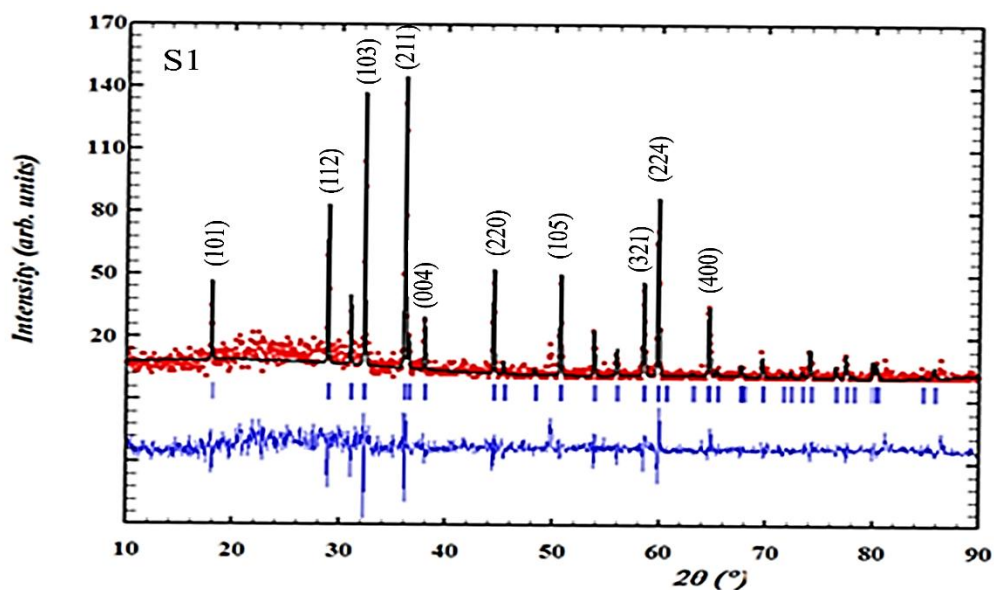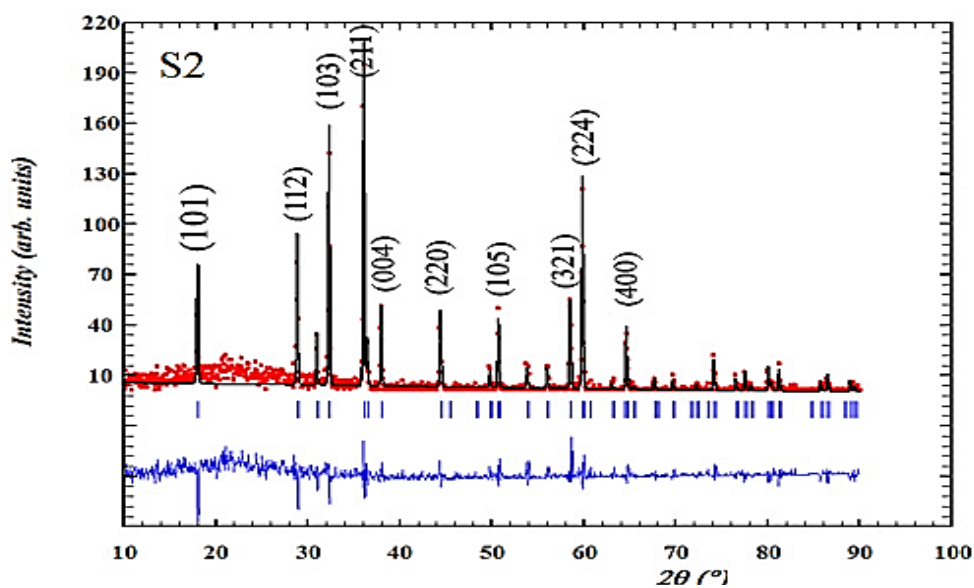
Figure 4a. *PXRD patterns of S₁.*

Figure 4b. *PXRD patterns of S₂.*

Table 1. *Cell parameters of samples S1 and S2 and tabulated values for Mn₃O₄. SD is the standard deviations.*

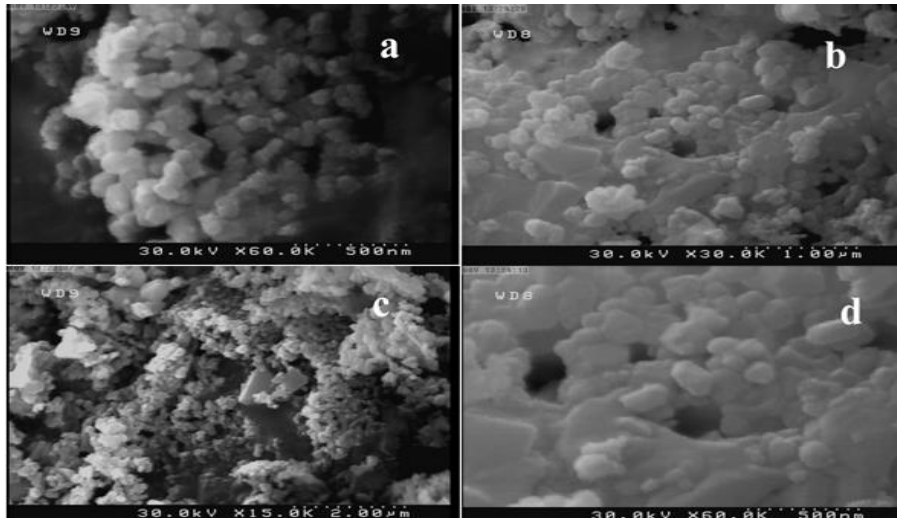| Sample	a (SD)	b (SD)	c (SD)	Volume (SD)
Standard sample (JCPDS 24-0734)	5.7621	5.7621	9.4696	314.408
S₁	5.7545(0.0066)	5.7545 (0.000)	9.4601(0013)	313.27(0.363)
S₂	5.7617 (0.0086)	5.7617 (0.000)	9.4658 (0.0017)	314.24 (0.471)

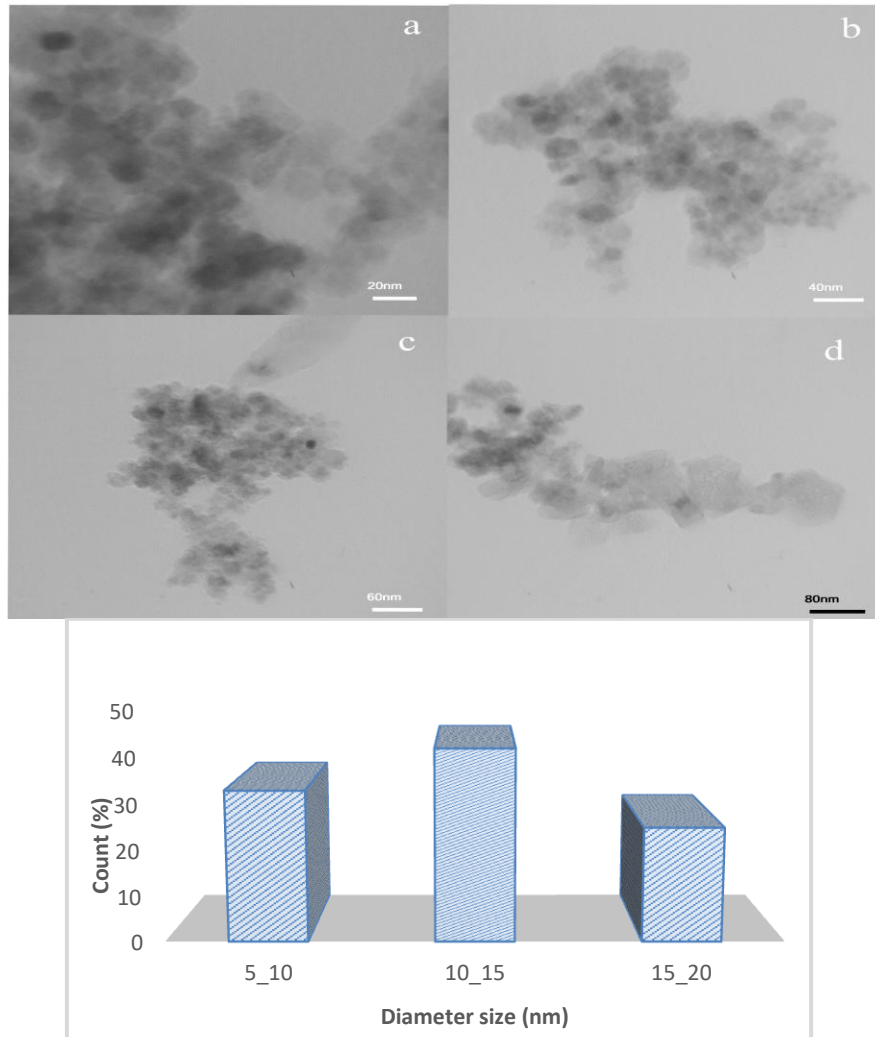***Figure 5.*** *FESEM images of S_1 and S_2.*

Figure 6. *TEM images (a-d) and particle size distribution profile of S_1.*

3.5. Magnetic Measurements

The magnetic hysteresis loops of synthesized Mn_3O_4 were investigated in a magnetic field range of -10 kOe to +60 kOe which is shown in Figure 7. It is observed that magnetization increases almost linearly with enhance of field that it is paramagnetic-like behavior, and does

Salehi and Ghasemi

not saturate even at the maximal applied field with the linear one in Figure 7 [24].
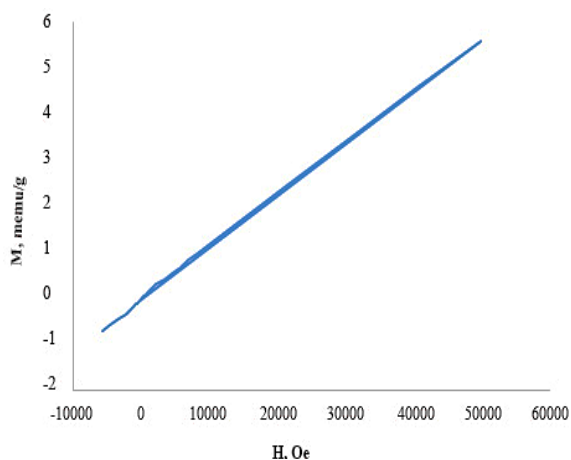
Figure 7. *Room temperature magnetic hysteresis loop of S_1 at a scan rate of 10 $mV\,s^{-1}$.*
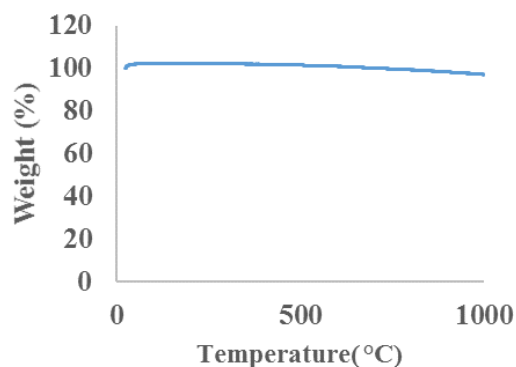
3.6. Thermal Analysis

Thermal stability of the final powder has been analyzed using TGA are presented in Figure 8 for S_1 and S_2. Calcined powder shows no weight loss, as all organic residues have been removed, that reveals the stability of obtained Mn_3O_4 nanoparticles.

4. CONCLUSIONS

In summary, nanostructured crystalline Mn_3O_4 was synthesized by a novel condition method. FESEM studies showed that the obtained nanomaterials had

Figure 8. *TGA thermograms of final powder after calcination of dried gel precursor.*

sphere-like structure. Also, SEM images showed that the synthesized nanomaterials were in different morphology that was dependent to the synthesis procedure. It is clear that reaction temperature is a main factor on the synthesized nanomaterial's morphologies. Cell parameter refinements, the magnetic measurement and thermal stability of the synthesized nanomaterials was investigated. The FTIR spectrum show the stretching and bending frequencies of the molecular group in the sample have been studied.

REFERENCES

1. Ozkaya T., Baykal A., Kavas H., Koseglu Y., Topark M. S. (2008). "A novel synthetic route to Mn_3O_4 nanoparticles and their magnetic evaluation", *Physica B*., 403: 3760-3764.
2. Santra S., Tapec R., Theodoropoulou N., Dobson J., Hebard A., Tan W. (2001). "Synthesis and Characterization of Silica-Coated Iron Oxide Nanoparticles in Microemulsion: The Effect of Nonionic Surfactants", *Langmuir*, 17: 2900-2906.
3. Gibot P., Laffont L., (2007). "Hydrophilic and hydrophobic nano-sized Mn_3O_4 particles", *J. Solid State Chem.*, 180: 695-701.
4. Han Y. F., Chen F., Zhong Z., Ramesh K., Chen L., Widjaja E., (2006). "Controlled Synthesis, Characterization, and Catalytic Properties of Mn_2O_3 and Mn_3O_4 Nanoparticles Supported on Mesoporous Silica SBA-15", *The Journal of Physical Chemistry*, 110: 24450-24456.
5. Tian Z. R., Tong W., Wang J. Y., Duan N. G., Krishnan V. V., Suib S. L., (1997). "Manganese Oxide Mesoporous Structures: Mixed-Valent Semiconducting Catalysts", *Science*, 276: 926-930.
6. Marbán G., Solís T. V., Fuertes A. B., (2004). "Mechanism of low-temperature selective catalytic reduction of NO with NH_3 over carbon-supported Mn_3O_4: Role of surface NH_3 species: SCR mechanism", *J. Catal.* 226: 138-155.
7. Yamashita T., Vannice A., (1997). "Temperature-programmed desorption of NO adsorbed on Mn_2O_3 and Mn_3O_4" *Appl. Catal. B: Environ.*, 13: 141-155.

8. Salari D., Niaei A., Hosseini S. A., Aleshzadeh R., Afshary H. (2010). "Investigation of the Activity of Nano Structure Mn/γ-Al$_2$O$_3$ Catalyst for Combustion of 2-Propanol", *Int. J. Nanosci. Nanotechnol.*, 6: 23-30.

9. Wang Y. J., Cheng L., Li F., Xiong H. M., Xia Y. Y., (2007). "High Electrocatalytic Performance of Mn$_3$O$_4$/Mesoporous Carbon Composite for Oxygen Reduction in Alkaline Solutions", *Chem. Mater.*, 19: 2095-2101.

10. Oaki Y., Imai H., Angew. (2007). "One-Pot Synthesis of Manganese Oxide Nanosheets in Aqueous Solution: Chelation-Mediated Parallel Control of Reaction and Morphology", *Chem. Int. Ed.*, 46: 4951-4955.

11. Salazar-Alvarez G., Sort J., Suriñach S., Baró M. D., Nogués J, (2007). "Synthesis and Size-Dependent Exchange Bias in Inverted Core−Shell MnO|Mn$_3$O$_4$ Nanoparticles", *J. Am. Chem. Soc.,* 129: 9102-9108.

12. Mohan G. R., Ravinder D., Ramana Reddy A. V., Boyanov B. S., (1999). "Dielectric properties of polycrystalline mixed nickel–zinc ferrites", *Materials Letters*, 40: 39-45.

13. Ovshinsky S. R., Fetcenko M. A., (1993). "A Nickel metal hydride battery for electric vehicles ", *Science*, 260: 176-181.

14. Sanchez L., Farcy J., Tirado J., (1996). "Low-temperature mixed spinel oxides as lithium insertion compounds", *J. Mater. Chem.*, 6: 37-39.

15. Thackeray M. M., David V. I. F., Bruce P. G., (1983). "Lithium insertion into manganese spinels", *Mater. Res. Bull.*, 18: 461-472.

16. Buckelew A., Galán-Mascarós J. R., Dunbar K. R., (2002). "Facile Conversion of the Face-Centered Cubic Prussian-Blue Material K$_2$[Mn$_2$(CN)$_6$] into the Spinel Oxide Mn$_3$O$_4$ at the Solid/Water Interface", *Advanced Materials*, 14: 1646-1648.

17. Chang Y. Q., Xu X. Y., Luo X. H., Chen C. P., Yu D. P., (2004). "Synthesis and characterization of Mn$_3$O$_4$ nanoparticles", *J. Cryst. Growth,* 264: 232-236.

18. Dahmardeh A., Davarpanah A. M., (2015). "Investigation on Influences of Synthesis Methods on the Magnetic Properties of Trimetallic Nanoparticles of Iron-Cobalt-Manganese Supported by Magnesium Oxide ", *Int. J. Nanosci. Nanotechnol.*, 11: 249-256.

19. Zhang Y. C., Qiao T., Hu X. Y., (2004). "Preparation of Mn$_3$O$_4$ nanocrystallites by low-temperature solvothermal treatment of γ-MnOOH nanowires", *J. Solid State Chem.*, 177: 4093-4097.

20. Apte S. K., Naik S. D., Sonawane R. S., Kale B. B., Pavaskar N., Mandale A. B., Das B. K., (2006). "Nanosize Mn$_3$O$_4$ (Hausmannite) by microwave irradiation method", *Mater. Res. Bull.,* 41: 647-654.

21. Chen Z. W., Lai J. K. L., Shek C. H., (2006). "Shape-controlled synthesis and nanostructure evolution of single-crystal Mn$_3$O$_4$ nanocrystals", *Scr. Mater.*, 55: 735-738.

22. Grootendorst E. J., Verbeek Y., Ponce V., (1995). "The Role of the Mars and Van Krevelen Mechanism in the Selective Oxidation of Nitrosobenzene and the Deoxygenation of Nitrobenzene on Oxidic Catalysts", *J. Catal.,* 157: 706-712.

23. Baldi M., Finonnhio E., Milella F., Busca G., (1998). "Catalytic combustion of C3 hydrocarbons and oxygenates over Mn$_3$O$_4$", *Appl. Catal. B: Environ.,* 16: 43-51.

24. Ozkaya T, Baykal A., Kavas H., Köseoğlu Y., Toprak M. S., (2008). "A novel synthetic route to Mn$_3$O$_4$ nanoparticles and their magnetic evaluation", *Physica B: Condensed Matter*, 403: 3760-3764.